IJMS
Vol 50, No 5, May 2025

Original Article

The Ameliorative Effect of Adipose-Derived Mesenchymal Stem Cells and Their Exosomes in Non-alcoholic Steatohepatitis by Simultaneously Enhancing Autophagic Flux and Suppressing Endoplasmic Reticulum Stress

Zahra Moayedfard[1,2], PhD; Kamran Bagheri Lankarani[3], MD; Ali Akbar Alizadeh[2], PhD; Ali Akbar Nekooeian[4], PhD; Mahintaj Dara[5], PhD; Farhad Koohpeyma[1,6], PhD; Shima Parsa[7], MD; Saman Nikeghbalian[8], MD; Arghavan Hosseinpouri[1,2], PhD; Negar Azarpira[7], MD

[1]Student Research Committee, Shiraz University of Medical Sciences, Shiraz, Iran;
[2]Department of Tissue Engineering and Applied Cell Sciences, School of Advanced Medical Sciences and Technologies, Shiraz University of Medical Sciences, Shiraz, Iran;
[3]Health Policy Research Center (HPRC), Shiraz University of Medical Sciences, Shiraz, Iran;
[4]Department of Pharmacology, School of Medicine, Shiraz University of Medical Sciences, Shiraz, Iran;
[5]Stem Cells Technology Research Center, Shiraz University of Medical Sciences, Shiraz, Iran;
[6]Endocrine and Metabolism Research Center, Shiraz University of Medical Sciences, Shiraz, Iran;
[7]Transplant Research Center, Shiraz University of Medical Sciences, Shiraz, Iran;
[8]Abu Ali Sina Hospital for Medicine and Organ Transplant, Shiraz University of Medical Sciences, Shiraz, Iran

Correspondence:
Negar Azarpira, MD;
Transplant Research Center, Shiraz University of Medical Sciences, Khalili Street, 7193711351, Shiraz, Iran
Tel: +98 71 36281439
Email: negarazarpira@yahoo.com
Received: 20 July 2024
Revised: 01 September 2024
Accepted: 22 September 2024

What's Known

- Several studies have been conducted on the pathology and effects of mesenchymal stem cells and their exosomes in various stages of non-alcoholic fatty liver disease, and their therapeutic effect has been proven to some extent.

What's New

- In this study, exosomes derived from adipose-derived mesenchymal stem cells significantly restored the autophagy process and suppressed the unfolded protein response pathways in the early stage of non-alcoholic fatty liver disease.

Abstract

Background: Due to the scarcity of treatment options, managing the progression of non-alcoholic fatty liver disease (NAFLD) from steatosis to cirrhosis necessitates innovative approaches. This study focused on endoplasmic reticulum (ER) stress, apoptosis, and autophagy as key mechanisms in NAFLD pathogenesis. It also highlighted the potential of adipose-derived mesenchymal stem cells (AD-MSCs) and their exosomes as promising therapeutic options.

Methods: The study was conducted at the Department of Regenerative Medicine, Shiraz University of Medical Sciences, (Shiraz, Iran) from November 2021 to December 2023. The mice (n=32) were divided into four groups: control, high-fat diet (HFD) without treatment, HFD with AD-MSCs treatment, and HFD with AD-MSCs-derived exosomes groups. The mice were fed HFD for 8 weeks. They received MSC and exosomes for the last 3 weeks. One week after the final injection, mice were tested for serum testing, stereological analysis, and real-time polymerase chain reaction (RT-PCR). The data were analyzed using the Graph-Pad Prism software by one-way analysis of variance (ANOVA) with Tukey analysis as a *post hoc* comparison between groups. $P<0.05$ indicated a significant difference.

Results: AD-MSCs-exosomes significantly reduced ER stress indicators (*IRE1α* [P=0.0001], *PERK* [P=0.0006], *ATF6* [P=0.0001], and *GRP78* [P=0.0001]), apoptosis markers (*Bax* [P=0.005] and *Cas3* [P=0.001]), and autophagic flux markers (*P62* [P=0.0001] and *LC3B/A* [P=0.003]).

Conclusion: In this investigation, AD-MSCs-exosomes significantly restored autophagy and suppressed unfolded protein response (UPR) pathways in the early stages of NAFLD.

Please cite this article as: Moayedfard Z, Bagheri Lankarani K, Alizadeh AA, Nekooeian AA, Dara M, Koohpeyma F, Parsa S, Nikeghbalian S, Hosseinpouri A, Azarpira N. The Ameliorative Effect of Adipose-Derived Mesenchymal Stem Cells and Their Exosomes in Non-alcoholic Steatohepatitis by Simultaneously Enhancing Autophagic Flux and Suppressing Endoplasmic Reticulum Stress. Iran J Med Sci. 2025;50(5):334-350. doi: 10.30476/ijms.2024.103376.3660.

Keywords ● Non-alcoholic fatty liver disease ● Mesenchymal stem cells ● Exosome ● Autophagy ● Endoplasmic reticulum stress

Introduction

Non-alcoholic fatty liver disease (NAFLD) is the hepatic manifestation of metabolic syndrome, defined by >5% hepatic

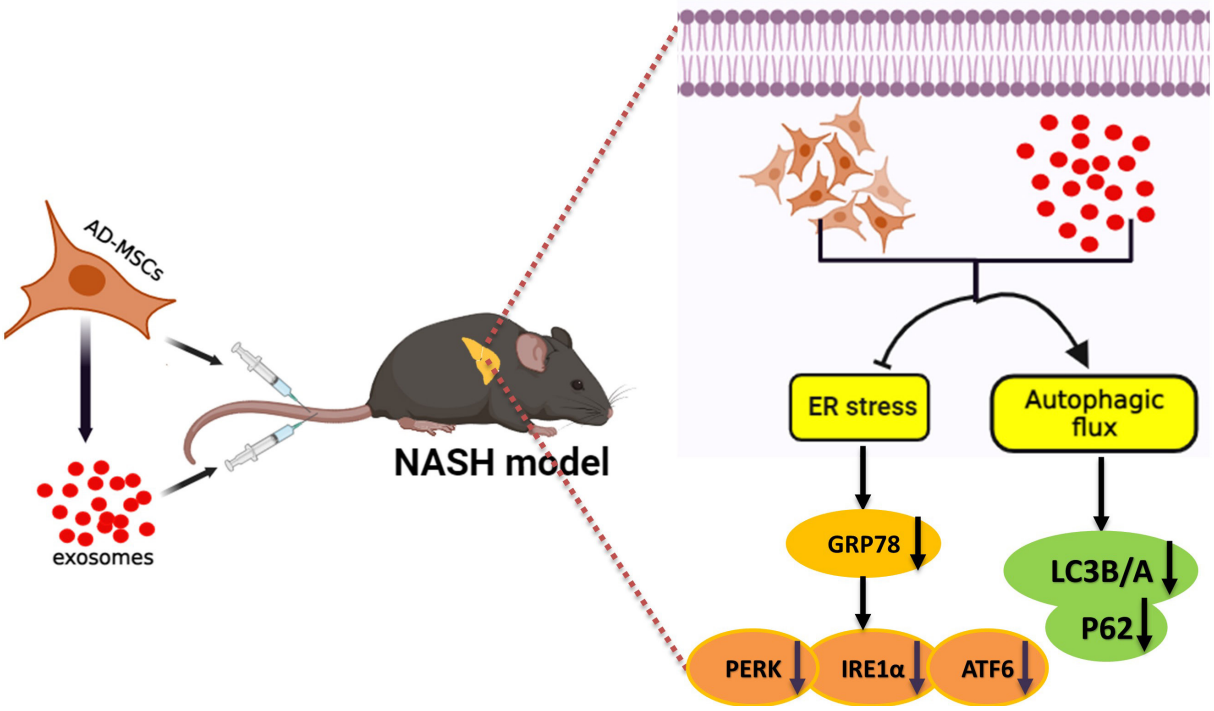

Graphical abstract: AD-MSCs and exosomes have a positive effect on NASH mice by restoring autophagic flux and suppressing ER stress in the early stages of NAFLD.

steatosis, with around 30% progressing to non-alcoholic steatohepatitis (NASH), which in around 20% of cases can advance to cirrhosis.[1] Despite its life-threatening consequences, NASH lacks a definitive therapeutic approach, making liver transplantation surgery the only available option for the cirrhosis condition.[2] Hence, investigating innovative and unrestricted treatment approaches based on their underlying impact mechanisms could be a focus of future research. Thus far, three primary mechanisms, including endoplasmic reticulum (ER) stress, apoptosis, and autophagy, have been proposed to play crucial roles in controlling the NASH process.[3, 4]

The accumulation of unfolded proteins in the endoplasmic reticulum (ER) leads to ER stress, which triggers the unfolded protein response (UPR) to restore ER balance. It is initially activated by ER chaperones and proteins that control protein quality, such as glucose-regulated protein 78 (*GRP78*).[5] The UPR pathway also regulates hepatic lipid metabolism.[6] Three ER trans-membrane stress sensors primarily manage it: inositol requiring enzyme1α (*IRE1α*), activating transcription factor 6 (*ATF6*), and protein kinase RNA-like ER kinase (*PERK*).[7]

Chronic or irreversible ER stress leads to cell apoptosis, with pro-apoptotic members of the *BCL-2* protein family members (such as *Bax*) and caspase3 playing a crucial role at the mitochondrial level by triggering the release of cytochrome c and the assembly of the apoptosome.[8]

Autophagy is a catabolic process that is genetically encoded and maintained throughout evolution. It involves breaking down damaged organelles and cellular proteins. It promotes cell survival and maintains cellular homeostasis. Several elements, such as the autophagy-related genes (*ATGs*), *p62*, the microtubule-associated protein 1 light chain 3 beta (*MAP1LC3*), and *Beclin 1*, play important roles in autophagic regulation.[9] *ATG* conjugates transform microtubule-associated proteins 1A/1B light chain 3A (*LC3B/A-I*) into *LC3 B/A -II*. This conversion is a crucial step in the maturation of autophagosomes, allowing them to fuse with lysosomes and break down the cargo inside the autophagosomes.[10] Under fat accumulating-induced stress, autophagy hydrolyzes fat droplets containing lipids.[11] In this regard, recent studies have suggested that an impaired autophagy pathway could be related to lipid accumulation within hepatocytes, causing hepatic steatosis.[12] Therefore, autophagy activation might be crucial for NAFLD control by alleviating the hepatic lipid burden. Conversely, an inadequate ER stress response triggers a cascade of steatosis, inflammation, autophagy, and apoptosis, all of which are hallmarks of NAFLD pathogenesis. Elucidating the agents that regulate these pathways holds promise for therapeutic development.[13]

Recent studies have shown that stem cell therapies, such as mesenchymal stem cells

(MSCs), could reduce liver inflammation and scarring, while also replenishing hepatocytes. In early clinical trials, they also have shown good tolerability and safety, as well as evidence of efficacy in liver failure patients.[14] However, MSC therapy may have potential downsides, including undesired lineage differentiation, limited engraftment, and the risk of malignant transformation.[15] Therefore, cell-free regenerative methods, such as applying extracellular vesicles (EVs), were introduced as more advantageous alternatives.[16]

EVs are membrane-bound particles released by various cell types and can be found in blood, urine, milk, and multiple tissues. Exosomes, a type of EVs, can be generated on a large scale using cells with a high proliferation potential, such as MSCs. Moreover, they have no definite side effects and can target specific tissues with a long circulation half-life.[17] Human umbilical cord MSC-derived exosomes could regenerate and repair damaged liver tissue in cases of liver injury.[16] Exosomes might contribute to liver injury repair by dampening α-smooth muscle actin (α-SMA) and collagen I expression, potentially through Kupffer and hepatic stellate cell inhibition. This could reduce inflammation, enhance liver function (AST/ALT), and stimulate hepatocyte regeneration.[18]

Previous *in vitro* studies have identified key pathways in NAFLD pathogenesis.[19, 20] However complementary *in vivo* studies are crucial to gain a better understanding of NAFLD pathogenesis, which hinders therapeutic development. Therefore, this study aimed to elucidate the mechanisms of NASH progression, with a focus on autophagy, endoplasmic reticulum stress, and apoptosis pathways. Besides, it investigated the therapeutic potential of adipose-derived mesenchymal stem cells (AD-MSCs) and their exosomes on these underlying pathways in NASH mice models induced by a high-fat diet.

Materials and Methods

Animals and Diet

Thirty-two male C57BL/6 mice, aged 6-8 weeks and weighing 16-18 g, were procured from the Laboratory Animal Breeding Center at Shiraz University of Medical Science. The Ethics Committee of Shiraz University of Medical Sciences (Shiraz, Iran) approved this study (code: IR.SUMS.REC.1399.860).

It was conducted following the National Institutes of Health guidelines for the care and use of laboratory animals (NIH Publications No. 8023, revised 1978).[21] The mice were housed under standard conditions, with a 12-hour light/dark cycle, 22-26 °C temperature range, and 25%-35% humidity. Throughout the study, the animals had free access to water and food.

Study Design

After 1 week of food adaptation, the mice were randomly divided into four groups, each consisting of eight. The four groups were the standard control group (control), the high-fat diet feeding group (NASH), the MSC intervention group (NASH+MSC), and the exosome intervention group (NASH+Exosome). The control group received a standard diet, while the other groups were given an HFD (59% standard feed+33% fat+2% cholesterol+1% cholate+5% sucrose) until the end of the experiment. In the 6th, 7th, and 8th weeks, 1×10^{6} MSC and 100 µg exosomes were injected intravenously through the tail in the (NASH+MSC) and (NASH+Exosome) groups. Following the final injection, the mice were given a week to recover before being euthanized. Blood and liver tissue samples were then randomly selected (figure 1).

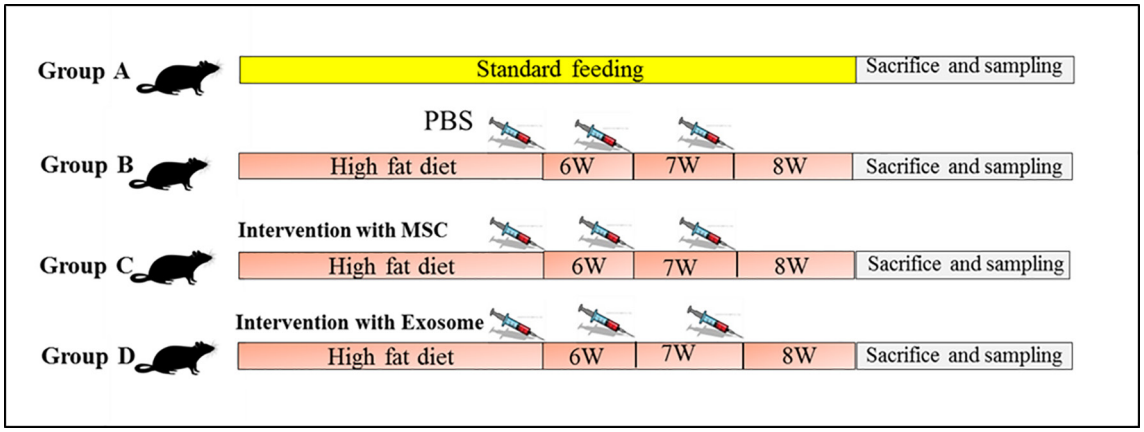

Figure 1: Study Design: Thirty-two mice were adapted to a diet for one week and then divided into four groups: group A (control), group B (NASH), group C (NASH+MSC), and group D (NASH+Exosome). The control group received standard feed, while the other groups were fed a high-fat diet. In the 6th, 7th, and 8th week, the NASH+MSC and NASH+Exosome groups were injected with 1×10^{6} MSC and 100µg exosome intravenously, (n=8). After a week of recovery, blood and liver tissue samples were collected for analysis.

The liver tissue samples were subsequently frozen in liquid nitrogen for molecular analysis and then transferred to -80 °C (n=5). The plasma was extracted from the blood samples to examine metabolic parameters and stored at -20 °C (n=5). The remaining liver tissue was stored in a 10% formalin solution (Sigma Aldrich, USA) for histological and stereological analysis (n=6). As the experimental and control groups were pre-defined, a blind intervention was not feasible. However, various other stages of the study, such as molecular and tissue analyses, were conducted randomly and blindly by different researchers.

Isolation of Mice AD-MSCs

Fine pieces of adipose tissue taken from a subcutaneous site of mice were subjected to digestion with 1 mg/mL collagenase IA (Sigma, USA) for 1 hour at 37 °C while shaking at a speed of 300 rpm. The digested tissue was then filtered using a Falcon® 100 µm Cell Strainer (SPL Life Sciences, Korea), centrifuged at 400 ×g for 5 min, and washed twice with phosphate-buffered saline (PBS) (Shellmax, Iran). The obtained cell pellet was suspended in an expanding medium, which consisted of DMEM/F12 medium with 10% fetal bovine serum (FBS), supplemented with penicillin (100 U/mL; Life Technologies, USA) and streptomycin (100 µg/mL; Life Technologies, USA). After resuspension, the tissues were seeded into a 25 cm culture flask (SPL Life Sciences, Korea) and incubated at 37 °C with 5% CO_2. The medium was renewed after 48 hours, and when the cell density reached 90%, they were detached using 0.25% trypsin/ethylene diamine tetra acetic acid for passage (EDTA) (Gibco, USA). Cells with good growth status at passage two or above were selected for further experiments.

Characterization of Mice AD-MSC

To conduct immunophenotyping on AD-MSCs, the cells were detached during passage three and then stained with Allophycocyanin (APC)-conjugated anti-mouse cluster of differentiation 44 (CD44), PerCP-cy5.5-conjugated anti-mouse CD105 and Phycoerythrin (PE)-conjugated anti-mouse CD73 antibodies from Beckman Coulter, USA (IM3630A), as well as Fluorescein isothiocyanate (FITC)-conjugated anti-mouse CD45 and PE-conjugated anti-mouse CD34 antibodies from eBioscience (CA, USA) in a dark environment for 40 min. Afterward, the samples were analyzed using fluorescence-activated cell sorting (FACS) Calibur from Becton Dickinson (San Jose, CA, USA) and Flowjo software from Tree Star (Ashland, USA).

Specific differentiation culture mediums were utilized to evaluate the ability of cultured AD-MSCs to differentiate into adipogenic and osteogenic cells. The cells were cultured until they reached approximately 80% confluence, and then they were exposed to an adipogenic or osteogenic induction medium for 21 days. Afterward, the cells were rinsed twice in PBS and fixed using a 4% paraformaldehyde solution (Merck, Germany). The fixed cells were stained with Oil Red-O and Alizarin Red using reagents (Sigma-Aldrich, USA).

Isolation of the Mice ADSCs-Exosome

After being washed with PBS, the cells were placed in a serum-free medium and cultured for 48 hours. The Exocib isolation kit (Exocib, Iran) was used to isolate exosomes from the cell medium, according to the manufacturer's protocols. The final product was stored at -80 °C for further examination.

Characterization of Mice ADSCs-Exosome

The size and morphology of the extracted exosomes were evaluated using transmission electron microscopy. Furthermore, flow cytometry was used to identify surface markers on the exosome membrane. To do this, magnetic beads were vortexed for 30 sec and mixed with 20 µL of exosomes containing 16µg. The mixture was then shaken for 24 hours on a shaker (Bio-Equip, China) at a temperature of 2-8 °C. After washing the tube with PBS, it was subjected to a magnetic field. The supernatant was then eliminated and replaced with 400µL of PBS. This procedure was performed twice. Next, the extracellular vesicles (ECV)-bead combination was transferred to flow cytometry tubes (BD Biosciences, UK) and supplemented with anti-CD9 and CD63 antibodies conjugated with PE (all obtained from BD Pharmingen™). The ECVs underwent analysis through a flow cytometer's fluorescence channels (FL2 and FL4) (BD FACS-Calibur-TM, BD Biosciences, UK), and the results were assessed using FlowJo software (Ashland, USA).

To determine the size of ECV, the exosomes were evaluated using a nanoparticle analyzer dynamic light scattering (DLS) (HORIBA, Japan) at an angle of 173° and had a wavelength of 532 nm. The measurements were taken at a fixed position and temperature of 25 °C in cuvettes. Three separate measurements were taken for each sample, and the mean values were calculated by analyzing three samples. A Bicinchoninic Acid (BCA) protein assay kit (ThermoFisher, USA) was used to determine the protein content of exosomes and assess drug loading capacity. The kit included a copper

reagent, a BCA reagent (ThermoFisher, USA), and a standard solution. A standard curve was developed to measure different concentrations of bovine serum albumin. The exosome samples and standard solutions were mixed with the reagents and incubated at 60 °C for 15 minutes. The NanoDrop™ spectrophotometer (ThermoScientific, USA) was used to measure the absorbance at 562 nm.

Labelling of AD-MSCs with 1,1'-dioctadecyl-3,3,3',3'-tetramethylindodicarbocyanine (DiD)

To label MSCs, 5 µM of DiD (Biotium, USA) was used. The staining process involved suspending 1×10^6 MSCs in 1 mL Dulbecco's Modified Eagle Medium (DMEM) (Shellmax, Iran) with 5 µM DiD for 20 min at 37 °C, 95% humidity, and 5% CO_2. The cells were then washed three times with PBS to remove any surplus. For the experiment, approximately 1×10^6 cells of AD-MSCs were labeled and injected into the tail vein of both the control and experimental animals. After 4 days, the mice were placed in a camera instrument (Kodak fx pro, USA) to trace the labeled cells using excitation 630 nm/emission 700 nm.

Analysis of Metabolic Parameters

After a period of fasting, the mice were sacrificed, and their blood was collected to measure levels of serum glucose, triglycerides (TG), total cholesterol (TC), LDL-c, HDL-c, alanine aminotransaminase (ALT), aspartate aminotransaminase (AST), and alkaline phosphatase (ALP). The levels were determined using a calorimetric method, an automatic analyzer device (A25) programmed with Spanish software, and a kit (Biosystem, Spain).

Histopathological Assessment

After collecting liver tissue samples from each mouse, they were preserved in 10% PBS formalin and later embedded in paraffin blocks. The blocks were then cut into slices of 3-4 µm thickness and stained with hematoxylin and eosin (H&E) for histological examinations. Additionally, liver sections were stained with Oil Red staining to evaluate fat deposition.

Stereological Assessment

The liver was weighed and measured using immersion before being preserved in 10% PBS formalin for a week. The liver was then divided into segments, five of which were randomly selected for stereological analysis. The orientation method was employed to obtain isotropic and uniformly random sections. A fractional volume (Vv) included hepatocytes, central veins, and sinusoids. The point-counting technique was used to determine the composition of the portal triad's internal structures, such as veins, arteries, and bile ductules:

Vv=P(structure)/p(reference).

In this context, P (structure) refers to the number of points that align with the structure profiles. In contrast, p (reference) represents the number of points within the reference area of liver tissue. The "director" method determined the number of nuclei in hepatocytes, with a final magnification of 3500. This method involves selecting cells randomly and uniformly.[22]

RNA Isolation and Quantitative Reverse Transcription

To perform polymerase chain reaction (PCR), the RNeasy Mini kit (Qiagen, Hilden, Germany) was used to extract total RNA from mice livers. Subsequently, 1 µg of the total RNA was converted into a cDNA kit (AddBio Co, South Korea). For PCR amplification, the reaction mixture was prepared with 1 µL of cDNA, 5 µL of Premix SYBR Green PCR mix (Amplicon, Denmark), 0.5 µL of each forward and reverse primers, and the reaction reached 3 µL by adding DEPS water. *GAPDH* messenger RNA was used as internal controls and amplified from the same samples. The process began with an initial denaturation at 95 °C for 2 min. Following that, a two-step cycle procedure was used: denaturation at 95 °C for 15 sec, then annealing and extension at 60 °C for 1 min. This cycle was repeated 40 times using a 7700 Sequence Detector from Applied Biosystems. Gene expression levels were determined using the comparative threshold cycle (ΔΔCt) method, with *GAPDH* serving as the endogenous control. The data were analyzed using the Sequence Detection Systems software from Applied Biosystems StepOne system (ThermoFisher Scientific, USA). Table 1 displays the primer sequences.

Statistical Analysis

The experiments were conducted, and the outcomes were reported as the mean±SD. Statistically significant differences between groups were determined using one-way ANOVA analyses of variance, and the Tukey test. The data were analyzed using the Graph-Pad Prism software (version 9; San Diego, USA). $P<0.05$ was considered statistically significant.

Results

Characterization of AD-MSCs

MSCs were isolated from mice adipose tissue and characterized through morphological properties and differentiation to adipocytes at passage 3.

Table 1: The primer sequences

Primers	Forward	Reverse
Beclin 1	TGAGGCGGAGAGATTGGA	AGGTGGCATTGAAGACATTGG
MAP-LC3b-a	AGCGAGTTGGTCAAGATCATC	CGTAGACCATGTAGAGGAATCC
MAP-LC3-b	AAGGGAAGTGATCGTCGCC	ATCTTGGTGGGGTGCTGC
SQSTM-1/p62	AGGCACAGAAGACAAGAGTAAC	GTCCAGTCATCGTCTCCTCC
GRP78	GGTCGGCATCGACTTGG	CCTGATCGTTGGCTATGATCTC
IRE1α	GGAGGCAAGAACAACGAAGG	GGCAGAGACTATCAGCAAAGG
PERK	CTGGCGAACCGGAGTCAC	TGCAGCGATTCGTCCATCTAA
ATF6	CCTCCAGTTGCTCCATCTCC	ACCAGTGACAGGCTTCTCTTC
Bcl2	CCGGGAGAACAGGGTATGATAA	TCCAGCATCCCACTCGTAG
Bax	CCAGCTCTGAACAGATCATGAAG	AAGGTCAGCTCAGGTGTCT
Cas3	CATACATGGGAGCAAGTCAGT	ATCCGTACCAGAGCGAGAT
GAPDH	AAGAGGGATGCTGCCCTTAC	ATCCGTTCACACCGACCTTC

MAP-LC3 or *LC3:* Microtubule-associated protein 1A/1B-light chain 3; *SQSTM-1/p62:* sequestosome-1; *IRE1α*: Inositol-requiring enzyme 1α; *PERK*: PKR-like ER kinase; *ATF6:* Activating transcription factor 6;*BAX: Bcl2* associated X protein; *BCL2:* B-cell lymphoma 2; *cas3: Caspase3*; *BECN: Beclin1*; and *GAPDH*: glyceraldehyde-3-phosphate dehydrogenase

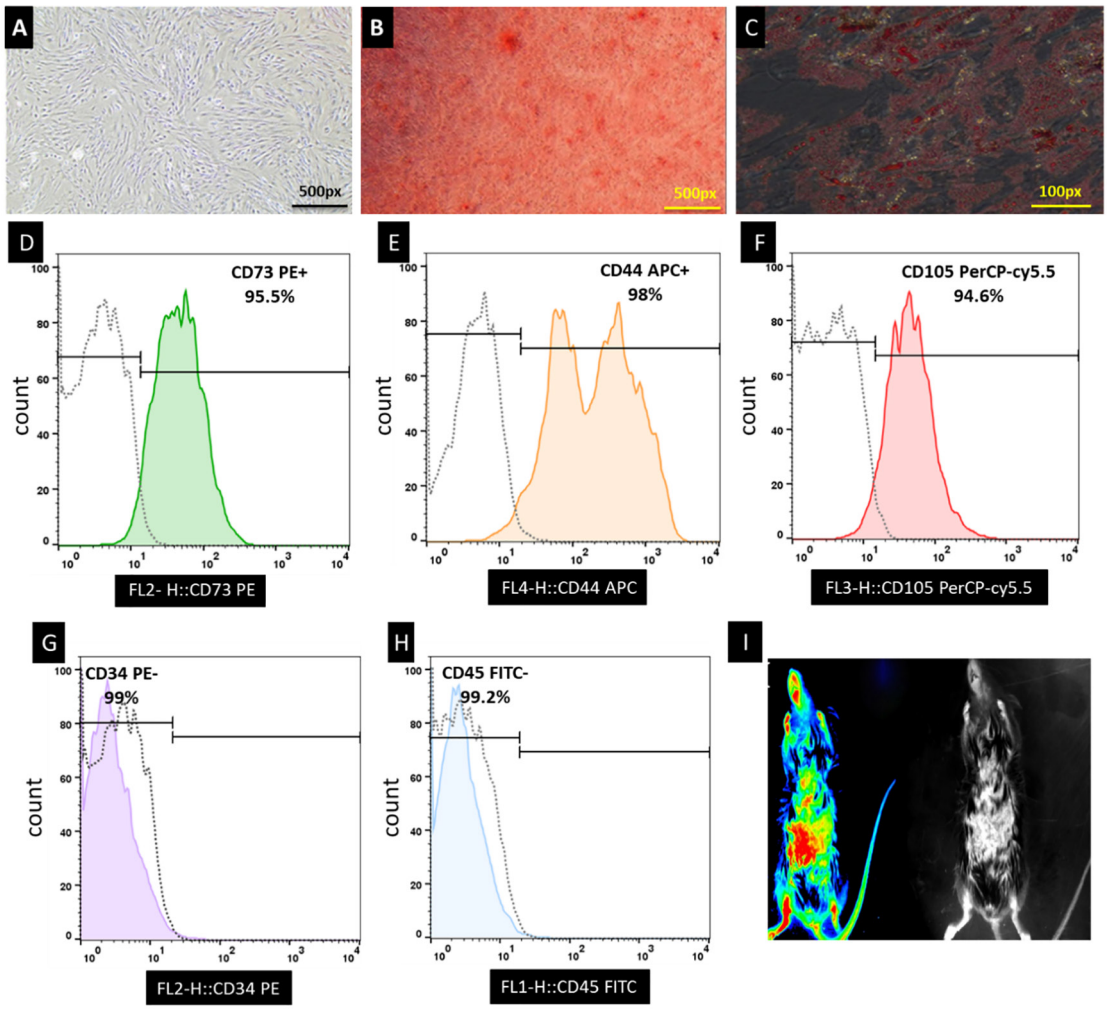

Figure 2: Characterization of ASCs is shown using histochemistry and flow cytometry. (A) The cells exhibit a homogeneous fibroblastic appearance. (B and C) The Alizarin Red and Oil Red-O Staining indicated the osteogenic and adipogenicity differentiation potential of ASCs. (D, E, and F, respectively) CD73, CD44, and CD105, mesenchymal stem cell surface markers were highly expressed. (G and H) CD45 and CD34, hematopoietic stem cell surface markers, indicated low expression. (I) The tracking of AD-MSCs to the liver is illustrated in 4 days after injection.

The cells had a spindle-like morphology (figure 2A), and their differentiation potency was determined by incubating them with adipogenic and osteogenic medium for 21 days, followed by evaluating their differentiation using Oil Red-O and Alizarin Red staining, respectively (figures 2B and 2C). In addition, the purity of MSCs was assessed using flow cytometry to identify specific surface markers.

It was found that 95.5%, 98%, and 94.6% of the isolated cells were positive for CD73, CD44, and CD105, known as MSC markers. However, they indicated no expression of surface markers for hematopoietic and epithelial cells, such as CD34 and CD45 (figures 2D, E, F, G, and H). Four days following injection, labeled cells were observed around the liver (figure 2I).

Characterization of AD-MSC-exosomes

The TEM images in figure 3A display exosomes of different sizes, each surrounded by a membrane and containing a uniform cytoplasm. DLS analysis revealed that these exosomes ranged in size from 50-100 nm (figure 3B). Furthermore, flow cytometry analysis revealed that 98% and 99.1% of exosomes were $CD9^+$ and $CD63^+$, respectively (figures 3D and 3E).

AD-MSCs and AD-MSC-exosomes relieve histopathological damage in HFD-induced NASH mice

The study aimed to confirm the effect of AD-MSCs and AD-MSC-exosomes on liver dysfunction, lipid profiles, and histopathological damage. Compared to the control group, the NASH group exhibited evidence of liver damage, abnormal cell morphology, and increased inflammatory cells. However, after administering AD-MSCs and AD-MSC-exosomes treatment, the symptoms of histopathological damage were significantly reduced. These findings suggested that these treatments could be a therapeutic approach to address such damage (figure 4).

Effect of AD-MSCs and AD-MSC-exosomes on Liver Weight and Volume in HFD-induced NASH Mice

The mean liver weight and volume in mice treated with AD-MSCs and AD-MSC-exosomes indicated no significant differences compared to the normal liver models. In contrast, samples affected by NASH rose significantly in weight and volume (P=0.016 and P=0.002, respectively). Furthermore, while the NASH group had a remarkable elevation in volume and Kupffer cell numbers (P=0.001 and P=0.011, respectively), AD-MSCs and AD-MSC-exosomes therapy had no significant differences in Kupffer cell numbers compared to the healthy liver. However, AD-MSCs treatment had a significant reduction in hepatocyte volume (P=0.001) (figure 5).

AD-MSCs and AD-MSC-exosomes Controlled Hepatic Inflammation and Hepatic Congestion Volume in HFD-induced NASH Mice

AD-MSCs demonstrated great potential in mitigating hepatic inflammation and congestion

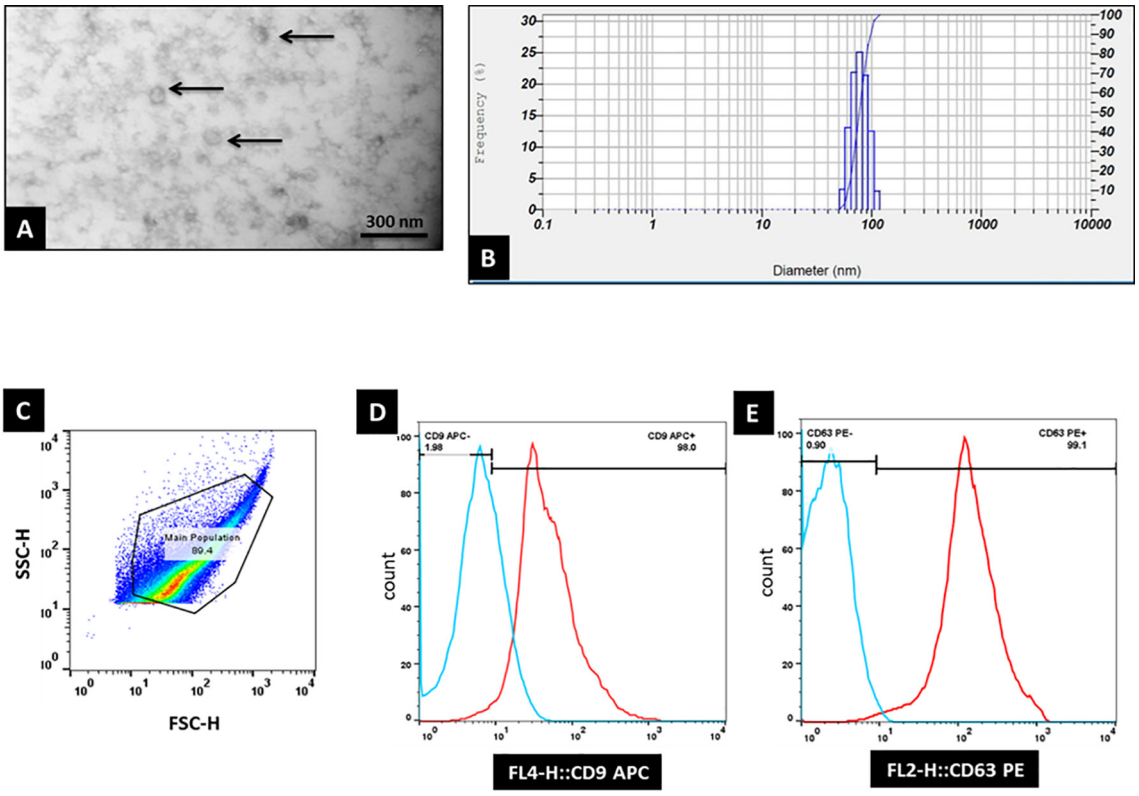

Figure 3: The characterization of AD-MSCs exosomes is illustrated. A) The black arrow indicates an exosome in a transmission electron microscopy image. B) Dynamic light scattering (DLS) results show the size range of these exosomes (50-100 nm). C) The main population of exosomes is shown. (D and E) The flow cytometry analysis of the exosomal surface markers CD9 and CD63 is also illustrated in the flow cytometry curve.

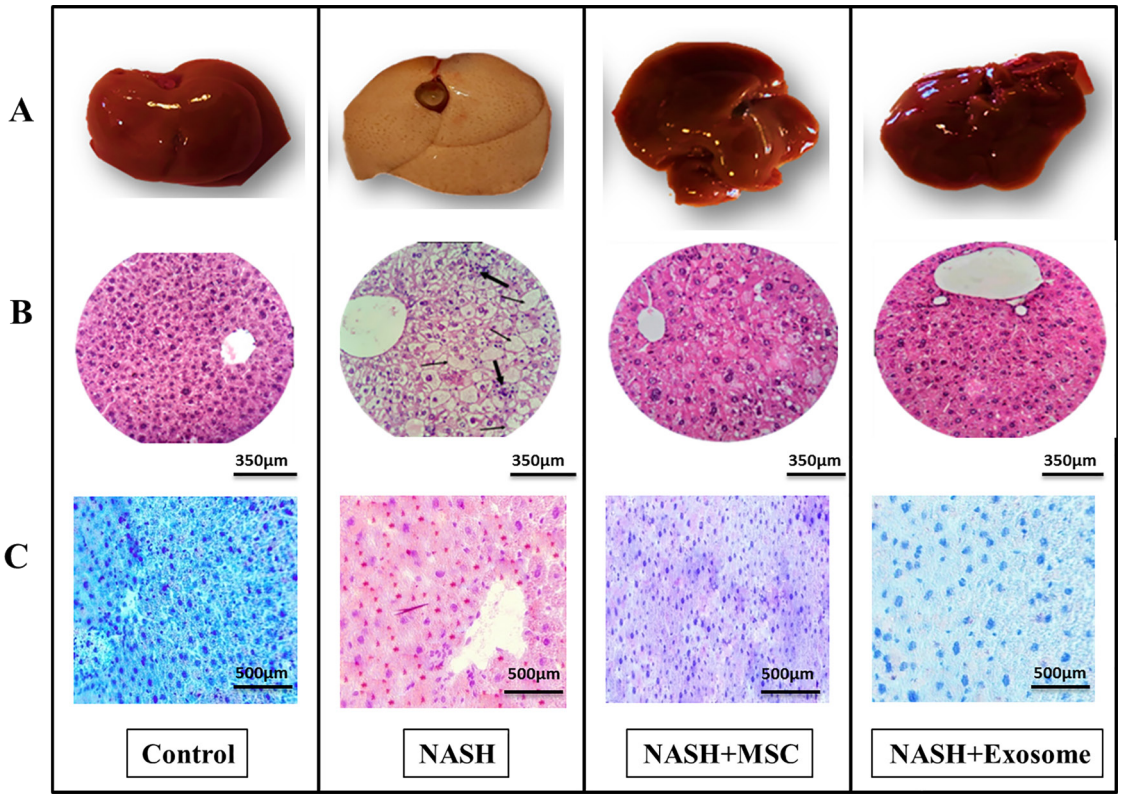

Figure 4: The effects of AD-MSCs and AD-MSC-derived exosome treatment in mice with HFD-induced steatohepatitis are illustrated. A) Photographs of liver appearances from different experimental groups are shown. B) Representative images of Hematoxylin and Eosin staining. C) Oil Red-O stained liver sections of the indicated groups are also shown.

(P=0.01 and P=0.001, respectively), while AD-MSC-exosomes exhibited an even stronger anti-inflammatory and congestion-reducing effect (P=0.001 and P=0.001, respectively). There was no significant difference between the therapeutic groups. Nonetheless, both significantly reduced hepatic steatosis volume, necrotic and fibrotic tissue volume, and cytoplasmic vacuolization volume (P=0.001, P=0.004, P=0.001, respectively). Notably, AD-MSC-exosomes significantly increased the volume of hepatocyte nuclei when compared to the NASH condition (P=0.012, figure 5).

AD-MSCs and AD-MSC-Exosome Alleviate Liver Dysfunction and Improve Lipid Profiles and FBS in HFD-induced NASH Mice

Mice with HFD-induced NASH had significantly higher liver enzyme levels (ALT, AST, and ALP) than the control group (P=0.0001 for all three enzymes). However, treatment with AD-MSCs and AD-MSC-exosomes significantly reduced these enzyme levels in respective groups as compared to the HFD-induced NASH group (P=0.0001 for all three enzymes). The HFD-induced NASH mice had significantly higher serum lipid profile levels (TC, TG, and LDL) than the control group (P=0.0001, P=0.002, and P=0.0001, respectively). However, treatment with AD-MSCs (P=0.0001, P=0.0001, and P=0.001, respectively) and AD-MSC-exosomes (P=0.0001 for all three enzymes) significantly reduced these levels (figure 6).

HDL levels were found to be lower in mice with HFD-induced NASH than in the control group (P=0.0001), whereas treatment with AD-MSCs and AD-MSC-exosomes significantly increased HDL levels (P=0.001 and P=0.005, respectively). This indicated that these treatments might improve liver function and lipid profiles in mice with HFD-induced NASH. On the other hand, FBS levels were higher in HFD-induced NASH mice than in the control group (P=0.0001). However, treatment with AD-MSCs (P=0.0005) and AD-MSC-exosomes led to a significant drop in FBS levels (P=0.001) (figure 6).

Effect of AD-MSCs and AD-MSCs-exosome Treatment on ER Stress Pathway Gene Expression

The RT-PCR analysis showed that the *GRP78* gene expression was significantly lower in the groups treated with AD-MSCs and AD-MSC-exosomes than in the NASH group (P=0.0001 for both). Moreover, the NASH-induced group exhibited a significant increase in *GRP78* expression than the healthy control group that received only PBS (P=0.0001). This study found

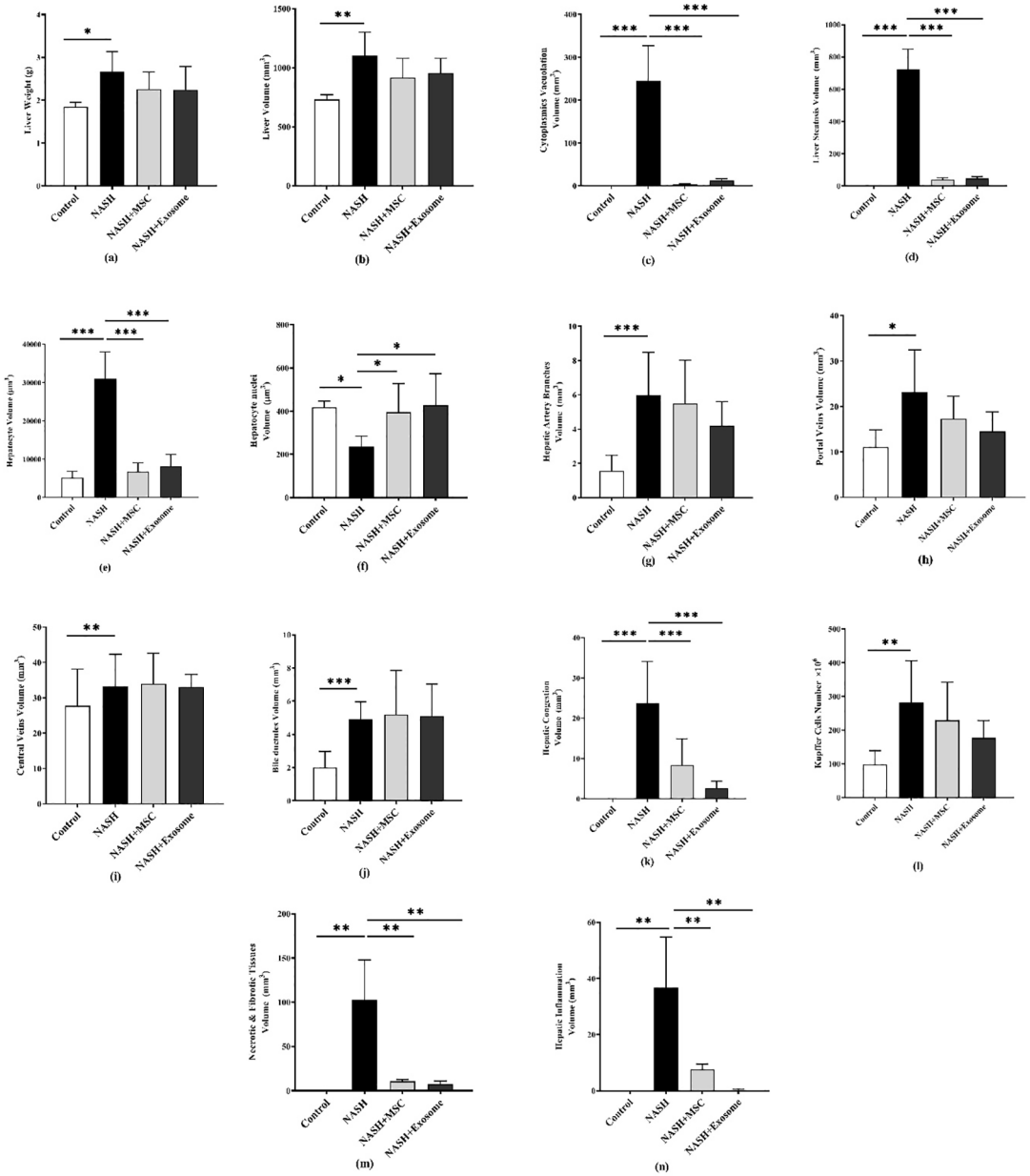

Figure 5: This figure shows how AD-MSCs and AD-MSC-derived exosomes affect stereology analysis. The data are presented as the mean±SD (n=6). The P values for the AD-MSCs and AD-MSC-derived exosome groups are as follows: Cytoplasmic vacuolation volume (P=0.001 for both groups), liver steatosis volume (P=0.001 for both groups), hepatocyte volume (P=0.001 for both groups), hepatocyte nuclei volume (P=0.012 for AD-MSCs group and P=0.0001 for the AD-MSC-derived exosome group), hepatic congestion volume (P=0.001 for both groups), necrotic and fibrotic tissues volume (P=0.004 for the AD-MSCs group and P=0.002 for the AD-MSC-derived exosome group). Lastly, for hepatic inflammation volume P=0.001 for both groups.

that *IRE1α* expression was significantly higher in the NASH group than in the control group (P=0.0002). However, treatment with AD-MSCs led to a significant decrease in *IRE1α* expression (P=0.0003), and treatment with AD-MSC-exosomes resulted in an even more substantial reduction (P=0.0001). Additionally, the expression of *PERK* mRNA was significantly higher in the NASH group than in the control group (P=0.019). However, treatment with NASH+MSC and NASH+Exosome significantly decreased *PERK* mRNA expression compared to the NASH group (P=0.013 and P=0.0006, respectively).

The NASH-induced group showed a significant increase in *ATF6* expression compared to the healthy control group that received only PBS (P=0.0002). However, both the AD-MSCs and AD-MSC-exosomes treatment groups had significantly lower expression of this gene than the NASH group (P=0.0006 and P=0.0001, respectively, figure 7).

Effect of AD-MSCs and AD-MSCs-exosome Treatment on Apoptosis Pathway Gene Expression

This study found that the expression of the *Bcl2* gene was significantly lower in the

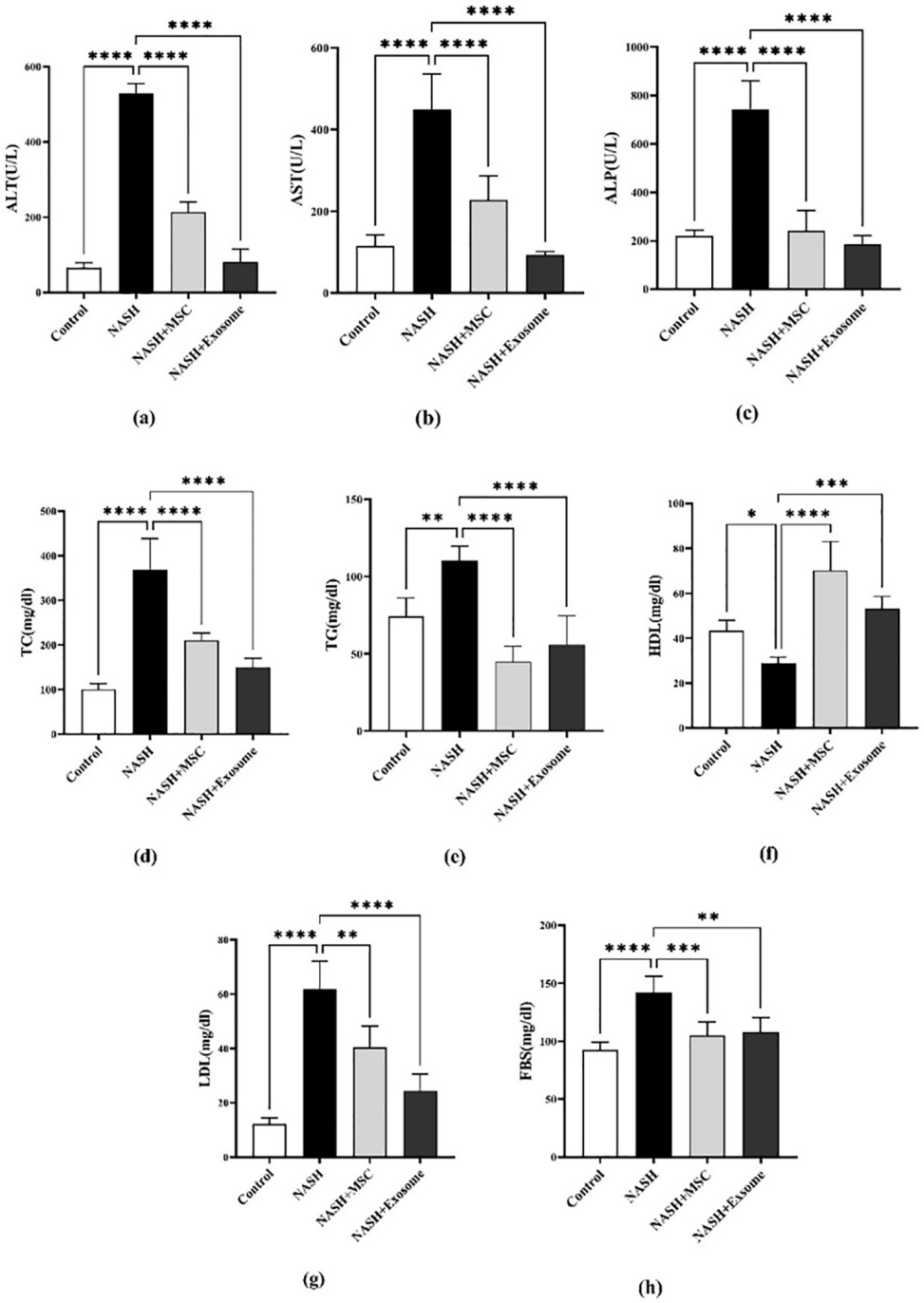

Figure 6: The effects of AD-MSCs and AD-MSCs-exosome on the levels of lipid profile, liver enzymes, and fasting blood sugar (FBS) in mice with HFD-induced non-alcoholic steatohepatitis (NASH) were investigated. The data are presented as the mean±SD (n=5). The P values for the AD-MSCs and AD-MSCs-exosome groups are presented as follows: For alanine aminotransferase (ALT), P=0.0001 for both groups; aspartate aminotransferase (AST), P=0.0001 for both groups; alkaline phosphatase (ALP), P=0.0001 for both groups. The lipid profile measurements included total cholesterol (TC), with P=0.0001 for both groups; triglycerides (TG), with P=0.0001 for both groups; high-density lipoprotein (HDL), with P=0.001 for the AD-MSCs group and P=0.005 for the AD-MSCs-exosome group; and low-density lipoprotein (LDL), with P=0.001 for the AD-MSCs group and P=0.0001 for the AD-MSCs-exosome group.

groups that received AD-MSCs and AD-MSC-exosomes than in the NASH group (P=0.0001 and P=0.0001, respectively). In contrast, the NASH group had a significantly higher expression level of Bcl2 mRNA than the control group (P=0.0001). The mice treated with AD-MSCs and AD-MSC-exosomes exhibited significantly lower expression of *Bax* than the NASH-induced mice (P=0.002 and P=0.005, respectively). The NASH-induced group had a significantly higher expression of *Bax* than the healthy control group (P=0.002). The study also revealed that *Cas3* expression was considerably higher in the NASH group than in the control group (P=0.0001).

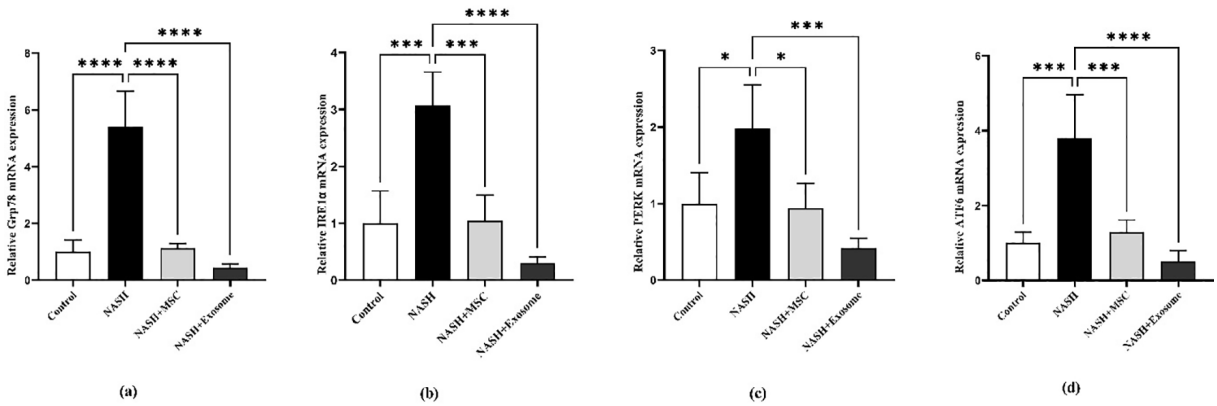

Figure 7: The effect of AD-MSCs and AD-MSCs-exosome treatment on the gene expression of the endoplasmic reticulum (ER) stress pathway was investigated. The data are presented as the mean±SD (n=4). The P values for the AD-MSCs and AD-MSCs-exosome groups are presented as follows: For *Grp78*, P=0.0001 for both groups; *IRE1α*, P=0.0003 for the AD-MSCs group and P=0.0001 for the AD-MSCs-exosome group; *PERK*, P=0.013 for the AD-MSCs group and P=0.0006 for the AD-MSCs-exosome group. Lastly, *ATF6*, P=0.0006 for the AD-MSCs group and P=0.0001 for the AD-MSCs-exosome group.

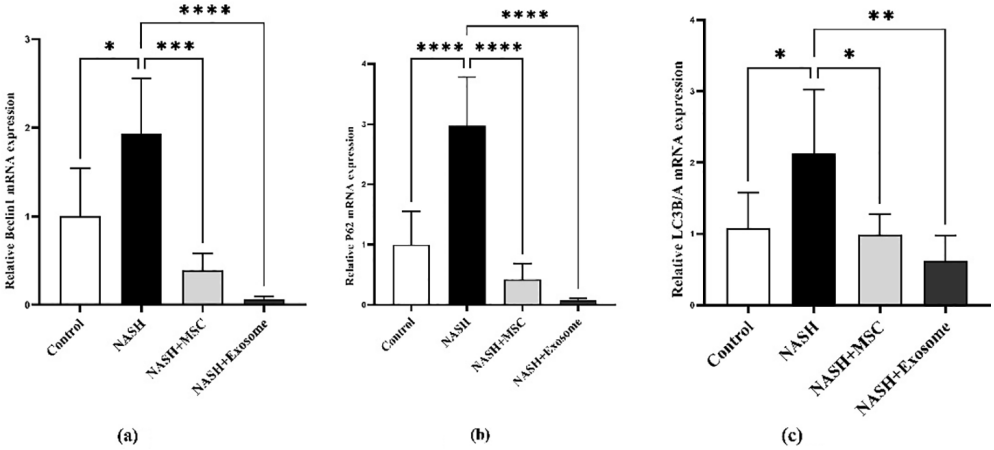

Figure 8: The effect of AD-MSCs and AD-MSCs-exosome treatment on the gene expression of the apoptosis pathway was studied. The results are presented as the mean±SD (n=5). The P values for the AD-MSCs and AD-MSCs-exosome groups are presented as follows: For *Bcl2*, P=0.0001 for both groups; for *Bax*, P=0.002 for the AD-MSCs group and P=0.005 for the AD-MSCs-exosome group; for *Cas3*, P=0.0001 for both groups.

However, administering AD-MSCs significantly reduced *Cas3* expression, and treatment with AD-MSC-exosomes showed a similar effect (P=0.0001 and P=0.0001, respectively); (figure 8).

Effect of AD-MSCs and AD-MSCs-exosome Treatment on Autophagy Pathway Gene Expression

The RT-PCR analysis revealed that the NASH group had significantly higher expression of the *Beclin1* gene than the control group (P=0.014). However, administering AD-MSCs and AD-MSC-exosomes resulted in a significant reduction in *Beclin1* mRNA expression in the NASH+MSC and NASH+Exosome groups compared to the NASH group (P=0.0001 and P=0.0001, respectively). The mRNA expression level of *p62* was considerably higher in the NASH group than in the control group (P=0.0001). Nevertheless, in the NASH+MSC and NASH+Exosome groups, the mRNA expression level of *p62* was significantly lower than that of the NASH group (P=0.0001 and P=0.0001, respectively). Furthermore, *LC3B/A* mRNA expression increased significantly in the NASH group compared to the control group (P=0.040). In contrast, *LC3B/A* mRNA expression levels were significantly lower in both the NASH+MSC group (P=0.024) and the NASH+Exosome group (P=0.003); (figure 9).

Effect of MSCs and Exosomes on Correlation of Beclin1, P62, LC3B/A, IRE1α, PERK, ATF6, Grp78, Bcl2, Bax, and Cas3 Genes

The correlation analysis of *Beclin1, P62, LC3B/A, IRE1, PERK, ATF6, Grp78, Bcl2, Bax*, and *Cas3* genes illustrated that most of these genes correlate 0-4 (figure 10). The heat map plot showed a grid structure representing the correlation between six genes across

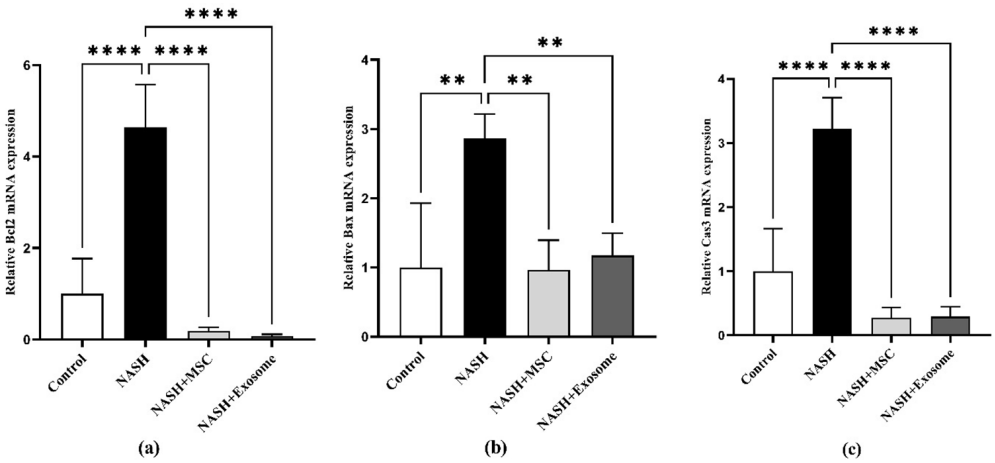

Figure 9: The impact of administering AD-MSCs and AD-MSCs-exosome on the gene expression of the autophagy pathway was investigated. The results are displayed as the mean±SD (n=4). The P values for the AD-MSCs and AD-MSCs-exosome groups are presented as follows: For *Beclin1*, P=0.0001 for both groups; for *p62*, P=0.0001 for both groups; for *LC3AB/A*, P=0.024 for the AD-MSCs group and P=0.003 for the AD-MSCs-exosome group.

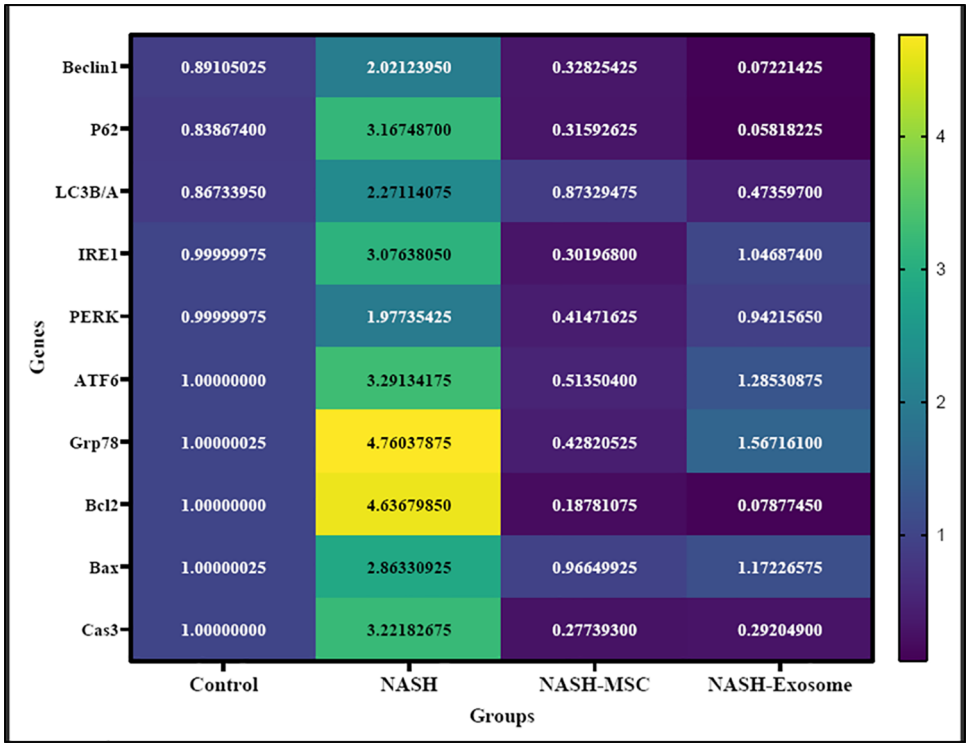

Figure 10: The effect of adipose-derived mesenchymal stem cells (AD-MSCs) and the treatment with exosomes derived from AD-MSCs on gene correlation is illustrated. Heat map plot showed the correlation of genes listed *Beclin1 P62, LC3B/A, IRE1, PERK, ATF6, Grp78, Bcl2, Bax*, and *Cas3* genes in control, NASH, NASH+MSC and NASH+ Exosome. The *ATF6*, *IRE1*, *P62*, and *Cas3* have a positive correlation with NASH (yellow to light green) and a negative correlation (light blue to dark blue) in NASH+MSC and NASH+Exosome groups.

four different groups. Each cell within the grid showed the correlation coefficient between the two intersecting genes and groups, with values ranging from 0-4, as indicated by the color scale on the right side of the heat map.

The color scale transitions ranged from dark blue (representing a correlation coefficient of 0-2) to green (representing a correlation coefficient of 2.0) to yellow (representing a correlation coefficient of 4.0). The darker yellow indicates a stronger positive correlation, while the darker blue indicates a stronger negative correlation between the gene pairs. Each row and column correspond to a specific gene and group, the heat map is annotated with correlation coefficients within each cell. The cells are color-coded based on the intensity and direction of the correlation. Many of the cells show negative correlations, as indicated by the hues of dark blue.

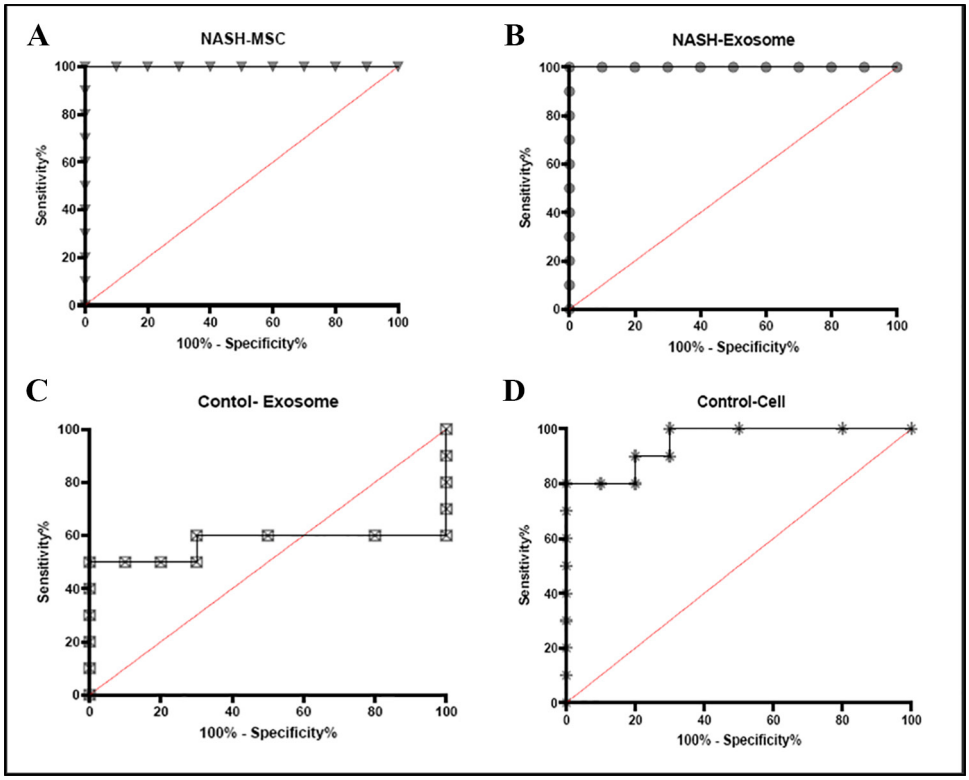

Figure 11: The specificity of genes in the NASH+MSC group (A) was higher than the NASH-Exosome group (B), as the area under the curve in A is bigger than in B. In addition, the studied genes were more sensitive to cell treatment than to exosome treatment. Furthermore, the NASH-Exosome group (B) and the NASH+MSC group (A) had a higher genes' specificity than the Control-MSC (D) and Control-Exosome (C) groups, based on the area under the curve.

ATF6, IRE, P62, and *Cas3* in the NASH group with green color showed a positive correlation. The genes expressed in the NASH-MSC and NASH-Exosome groups had a negative correlation with light blue to dark blue, while these genes in the NASH group had a negative correlation with yellow to light green, which could be attributed to the effect of MSC and exosomes in decreasing the expression level of these genes.

The effect of AD-MSCs and AD-MSCs-exosome treatment on gene correlation was investigated. The heat map plot illustrated the correlation of the following genes: *Beclin1, P62, LC3B/A, IRE1, PERK, ATF6, Grp78, Bcl2, Bax*, and *Cas3* in the control, NASH, NASH+MSC, and NASH+Exosome groups. The genes *ATF6, IRE1, P62,* and *Cas3* exhibited a positive correlation with NASH, as indicated by the colors ranging from yellow to light green. In contrast, these genes showed a negative correlation in the NASH+MSC and NASH+Exosome groups, as indicated by colors ranging from light blue to dark blue.

Evaluation of the Sensitivity/Specificity of Gene Markers to Cell and Exosome

A receiver operating characteristic (ROC) curve is a graphic representation that uses the false positive rate (specificity) on the X-axis and the true positive rate (sensitivity) on the Y-axis. It is generated by plotting these rates at different thresholds (different cut-off points). In this experiment, we compared the specificity and sensitivity of Control-NASH+Exosome, Control-NASH+MSC, NASH-NASH+MSC, and NASH-NASH+Exosome groups toward the gene expression tests. The specificity and sensitivity of the genes in the NASH+Exosome and NASH+MSC groups (figure 11 A and B) were completely higher than the Control-MSC and Control-Exosome groups (figure 11 C and D), as the area under the curve in figure 11 A and B was larger than in figure 11 C and D. Furthermore, in the Control+MSC and the Control+Exosome groups (figure 11 C and D), the low specificity of the genes was associated with high genes sensitivity. This early increase in gene sensitivity might indicate a general response to the treatment in the Control+MSC and Control+Exosome groups. Later, the genes that respond might become more specific to the treatment itself.

Discussion

The NASH-induced group had significantly higher

levels of mRNA expression for key regulators of the unfolded protein response (UPR) pathway, such as *GRP78*, *PERK*, *IRE1α*, and *ATF6*. Treatment with MSC-exosomes significantly suppressed the UPR pathway. These findings were consistent with previous *in vivo* studies that showed MSC-exosome administration affected ER stress-induced apoptosis and progression of intervertebral disc degeneration in a rat tail model.[23] In this regard, Lee and others suggested that MSCs could alleviate the ER stress response within the *PERK-Nrf2* signaling, leading to decreased expression of ER stress markers.[24] Additionally, after implanting BM-MSCs into rats with NAFLD, the expression of *ATF4* and *CHOP* was reduced.[25] Treatment with MSCs in palmitic acid-induced hepatocytes also resulted in a decrease in *CHOP* expression.[26] When ER stress becomes irreversible, the UPR can trigger various pathways, including the inflammatory response and apoptosis.[13] Notably, the application of MSC-exosomes in this study confirmed their significant potential to reduce liver inflammation, which could be closely related to a decrease in cytoplasmic vacuolization, liver steatosis, and the volume of necrotic and fibrotic tissue in NASH. These findings were consistent with previous *in vivo* and *in vitro* studies that demonstrated the anti-inflammatory properties of exosomes derived from bone marrow MSCs, umbilical cord-derived MSCs, AD- MSCs, and amnion-derived MSCs extracellular vesicles.[27-29] Furthermore, we observed a significant reduction in Kupffer cells following MSC-exosomes therapies in NASH models. The anti-inflammatory properties of MSCs, and more importantly, their derived exosomes, are likely associated with the suppression of Kupffer cells' activation and hepatic stellate cells, which are the key factors contributing to liver inflammation and excessive extracellular matrix production, both of which can lead to NAFLD. It was also implied that there was a correlation between these changes and a measurable increase in liver mass.[18, 27] Highlighting the role of inflammatory factors, Madpour and others suggested that an over-generation in anti-inflammatory cytokines (such as *TGF-β* and *IL-10*) and decreasing *IFN-γ* through MSCs-derived extracellular vesicles could reduce apoptosis progression in liver injury models.[30] Chen and others demonstrated the direct anti-apoptotic effects of MSC-conditioned medium (MSC-CM) in a radiation-induced liver injury model via modulating the inflammatory response, which was consistent with our findings on the anti-apoptotic impact of MSC-exosomes.[31] This agreement supported the observed down-regulation of the apoptosis markers, *Bax*, and *Cas3* mRNA in the MSC-exosomes group, suggesting a potential therapeutic function for this agent in NAFLD pathogenesis.

The findings of the present study supported impaired autophagic flux in the NASH group, as evidenced by the accumulation of *Beclin-1*, *P62*, and *LC3B/A* mRNA. *P62*, a ubiquitin-binding scaffold protein, clearly aggregates in liver injuries.[32] Under normal conditions, *p62* interacts with *LC3*, a critical autophagic protein, to facilitate the degradation of damaged organelles and protein aggregates by autophagy. However, impaired autophagic flux in NASH likely hinders *p62* degradation, leading to its accumulation alongside other autophagic markers (LC3B/A). This observation suggested a potential therapeutic effect of MSC-exosomes on NASH by significantly reducing autophagic-related variables such as *Beclin1, p62, and LC3AB/A*. This suggested the role of MSC-exosomes in autophagic flux restoration. In line with this finding, previous studies reported that MSCs promoted autophagy flux in acute liver injury, mainly through enhanced autophagy lysosomal fusion in the final stage. The same research identified exosomal let-7a-5p derived from MSCs as a critical contributor to their pro-autophagic effects. Let-7a-5p targets MAP4K3, which ultimately promotes the nuclear localization of transcription factor EB (TFEB).[33] This is further supported by an *in vivo* study, which suggested that mesenchymal stem cell exosomes activated autophagy pathway expression and played a protective role against inflammation in intervertebral disc degeneration in rat models.[34] Another study by Park and others discovered that mesenchymal stem cells from tonsils had the autophagy activating capacity to reduce liver damage brought on by CCl4 in rodents.[35] Besides, Hua and others discovered that human amniotic MSCs (hAMSCs) had the capacity to modify autophagy in livers treated with acetaminophen. This modulation leads to the suppression of M1 polarization and the promotion of M2 polarization of Kupffer cells (KCs), ultimately resulting in the alleviation of liver injury.[36] Furthermore, the therapeutic effect of MSCs was found to be weakened by using an autophagy inhibitor.[37]

In this study, it was further demonstrated that the serum levels of hepatic damage-related enzymes, total TG, and cholesterol were significantly higher in the liver-injured mice. At the same time, MSC-exosomes treatment significantly improved the condition. These findings were consistent with previous studies indicating that MSC-exosomes reduced liver-related inflammation and serum lipid profile enzymes.[38]

Indeed, the present study strongly highlighted the therapeutic potential of AD-MSC-exosomes for NASH. Compared to their cellular source, these exosomes provide distinct advantages over their biological source. Their smaller size facilitated production, storage, and delivery, making them a more straightforward and scalable therapeutic option. Additionally, the lack of viable cells eliminates tumor formation risk and reduces immunogenicity, potentially leading to safer and more predictable treatment outcomes. These combined effects, which were consistent with previous research, position AD-MSC-exosomes as a highly promising and translatable strategy for treating liver diseases such as NASH.[39]

This investigation had some limitations. For instance, although the HFD mouse is the most suitable animal model for NASH, it takes quite a long time and does not precisely mirror human conditions. Furthermore, the contents of the exosomes have not yet been fully explored.

Conclusion

The findings of the present study in a mouse model of NAFLD induced by a high-fat diet suggested that there was a preexisting link between ER stress and autophagy suppression, which could be alleviated through treatment with MSC exosomes. In this study, AD-MSC-exosomes significantly restored autophagic flux and suppressed UPR pathways during the early stages of NAFLD. This therapeutic approach showed promise for ameliorating NAFLD progression to more severe liver pathologies and ultimately enhancing hepatic function.

Similar investigations should be conducted using non-animal models such as organ on chip. The findings of this study required to be confirmed in future clinical trials before being used as a medicine to treat NASH.

Acknowledgment

The authors would like to thank the Council for Development of Regenerative Medicine and Stem Cells Technologies. This study was financially supported by the Research Deputy of Shiraz University of Medical Sciences (Grant no: 98-01-74-21114).

Authors' Contribution

Z.M: Study design, performing the study, and drafting the manuscript; K.BL: Study concept and reviewing the manuscript; AA.A: Study concept and reviewing the manuscript; AA.N: Data gathering, and reviewing the manuscript; M.D: Data gathering and reviewing the manuscript; F.K: Data analysis and drafting; Sh. P: Data analysis and drafting; S.N: Study concept and reviewing the manuscript; A.H: Data gathering and reviewing the manuscript, N.A: Study design, performing the study, and drafting the manuscript; All authors actively participated in drafting, reviewing, and finalizing the manuscript. All authors have read and approved the final manuscript and agree to be accountable for all aspects of the work in ensuring that questions related to the accuracy or integrity of any part of the work are appropriately investigated and resolved.

Conflict of Interest: None declared.

References

1 Rinaldi L, Pafundi PC, Galiero R, Caturano A, Morone MV, Silvestri C, et al. Mechanisms of Non-Alcoholic Fatty Liver Disease in the Metabolic Syndrome. A Narrative Review. Antioxidants (Basel). 2021;10. doi: 10.3390/antiox10020270. PubMed PMID: 33578702; PubMed Central PMCID: PMCPMC7916383.

2 Tsochatzis EA, Bosch J, Burroughs AK. Liver cirrhosis. Lancet. 2014;383:1749-61. doi: 10.1016/S0140-6736(14)60121-5. PubMed PMID: 24480518.

3 Lebeaupin C, Vallee D, Hazari Y, Hetz C, Chevet E, Bailly-Maitre B. Endoplasmic reticulum stress signalling and the pathogenesis of non-alcoholic fatty liver disease. J Hepatol. 2018;69:927-47. doi: 10.1016/j.jhep.2018.06.008. PubMed PMID: 29940269.

4 Wu WKK, Zhang L, Chan MTV. Autophagy, NAFLD and NAFLD-Related HCC. Adv Exp Med Biol. 2018;1061:127-38. doi: 10.1007/978-981-10-8684-7_10. PubMed PMID: 29956211.

5 Chen X, Shi C, He M, Xiong S, Xia X. Endoplasmic reticulum stress: molecular mechanism and therapeutic targets. Signal Transduct Target Ther. 2023;8:352. doi: 10.1038/s41392-023-01570-w. PubMed PMID: 37709773; PubMed Central PMCID: PMCPMC10502142.

6 Moncan M, Mnich K, Blomme A, Almanza A, Samali A, Gorman AM. Regulation of lipid metabolism by the unfolded protein response. J Cell Mol Med. 2021;25:1359-70. doi: 10.1111/jcmm.16255. PubMed PMID: 33398919; PubMed Central PMCID: PMCPMC7875919.

7 Mostafa RG, El-Aleem Hassan Abd El-Aleem A, Mahmoud Fouda EA, Ahmed Taha FR, Amin Elzorkany KM. A pilot study on gene expression of endoplasmic reticulum unfolded protein response in chronic kidney disease.

Biochem Biophys Rep. 2020;24:100829. doi: 10.1016/j.bbrep.2020.100829. PubMed PMID: 33134564; PubMed Central PMCID: PMCPMC7588702.
8 Iurlaro R, Munoz-Pinedo C. Cell death induced by endoplasmic reticulum stress. FEBS J. 2016;283:2640-52. doi: 10.1111/febs.13598. PubMed PMID: 26587781.
9 Gomez-Virgilio L, Silva-Lucero MD, Flores-Morelos DS, Gallardo-Nieto J, Lopez-Toledo G, Abarca-Fernandez AM, et al. Autophagy: A Key Regulator of Homeostasis and Disease: An Overview of Molecular Mechanisms and Modulators. Cells. 2022;11. doi: 10.3390/cells11152262. PubMed PMID: 35892559; PubMed Central PMCID: PMCPMC9329718.
10 Li X, He S, Ma B. Autophagy and autophagy-related proteins in cancer. Mol Cancer. 2020;19:12. doi: 10.1186/s12943-020-1138-4. PubMed PMID: 31969156; PubMed Central PMCID: PMCPMC6975070.
11 Xie Y, Li J, Kang R, Tang D. Interplay Between Lipid Metabolism and Autophagy. Front Cell Dev Biol. 2020;8:431. doi: 10.3389/fcell.2020.00431. PubMed PMID: 32582708; PubMed Central PMCID: PMCPMC7283384.
12 Zhang Y, Li K, Kong A, Zhou Y, Chen D, Gu J, et al. Dysregulation of autophagy acts as a pathogenic mechanism of non-alcoholic fatty liver disease (NAFLD) induced by common environmental pollutants. Ecotoxicol Environ Saf. 2021;217:112256. doi: 10.1016/j.ecoenv.2021.112256. PubMed PMID: 33901779.
13 Lee S, Kim S, Hwang S, Cherrington NJ, Ryu DY. Dysregulated expression of proteins associated with ER stress, autophagy and apoptosis in tissues from nonalcoholic fatty liver disease. Oncotarget. 2017;8:63370-81. doi: 10.18632/oncotarget.18812. PubMed PMID: 28968997; PubMed Central PMCID: PMCPMC5609929.
14 Cao Y, Ji C, Lu L. Mesenchymal stem cell therapy for liver fibrosis/cirrhosis. Ann Transl Med. 2020;8:562. doi: 10.21037/atm.2020.02.119. PubMed PMID: 32775363; PubMed Central PMCID: PMCPMC7347778.
15 Volarevic V, Nurkovic J, Arsenijevic N, Stojkovic M. Concise review: Therapeutic potential of mesenchymal stem cells for the treatment of acute liver failure and cirrhosis. Stem Cells. 2014;32:2818-23. doi: 10.1002/stem.1818. PubMed PMID: 25154380.
16 Pan Y, Tan WF, Yang MQ, Li JY, Geller DA. The therapeutic potential of exosomes derived from different cell sources in liver diseases. Am J Physiol Gastrointest Liver Physiol. 2022;322:G397-G404. doi: 10.1152/ajpgi.00054.2021. PubMed PMID: 35107032; PubMed Central PMCID: PMCPMC8917924.
17 Kumar MA, Baba SK, Sadida HQ, Marzooqi SA, Jerobin J, Altemani FH, et al. Extracellular vesicles as tools and targets in therapy for diseases. Signal Transduct Target Ther. 2024;9:27. doi: 10.1038/s41392-024-01735-1. PubMed PMID: 38311623; PubMed Central PMCID: PMCPMC10838959.
18 Ohara M, Ohnishi S, Hosono H, Yamamoto K, Yuyama K, Nakamura H, et al. Extracellular Vesicles from Amnion-Derived Mesenchymal Stem Cells Ameliorate Hepatic Inflammation and Fibrosis in Rats. Stem Cells Int. 2018;2018:3212643. doi: 10.1155/2018/3212643. PubMed PMID: 30675167; PubMed Central PMCID: PMCPMC6323530.
19 He Y, Yang W, Gan L, Liu S, Ni Q, Bi Y, et al. Silencing HIF-1alpha aggravates non-alcoholic fatty liver disease in vitro through inhibiting PPAR-alpha/ANGPTL4 singling pathway. Gastroenterol Hepatol. 2021;44:355-65. doi: 10.1016/j.gastrohep.2020.09.014. PubMed PMID: 33272734.
20 Sani F, Soufi Zomorrod M, Azarpira N, Soleimani M. The Effect of Mesenchymal Stem Cell-Derived Exosomes and miR17-5p Inhibitor on Multicellular Liver Fibrosis Microtissues. Stem Cells Int. 2023;2023:8836452. doi: 10.1155/2023/8836452. PubMed PMID: 37576406; PubMed Central PMCID: PMCPMC10421706.
21 Care IoLARCo, Animals UoL. Guide for the care and use of laboratory animals. US Department of Health and Human Services: Public Health Service, National Institutes of Health; 1986.
22 Bordbar H, Soleymani F, Nadimi E, Yahyavi SS, Fazelian-Dehkordi K. A Quantitative Study on the Protective Effects of Resveratrol against Bisphenol A-induced Hepatotoxicity in Rats: A Stereological Study. Iran J Med Sci. 2021;46:218-27. doi: 10.30476/ijms.2020.83308.1233. PubMed PMID: 34083854; PubMed Central PMCID: PMCPMC8163701
23 Liao Z, Luo R, Li G, Song Y, Zhan S, Zhao K, et al. Exosomes from mesenchymal stem cells modulate endoplasmic reticulum stress to protect against nucleus pulposus cell death and ameliorate intervertebral disc degeneration in vivo. Theranostics. 2019;9:4084-100. doi: 10.7150/thno.33638. PubMed PMID: 31281533; PubMed Central PMCID: PMCPMC6592170.
24 Lee EJ, Cardenes N, Alvarez D, Sellares J, Sembrat J, Aranda P, et al. Mesenchymal stem cells reduce ER stress via PERK-Nrf2

pathway in an aged mouse model. Respirology. 2020;25:417-26. doi: 10.1111/resp.13646. PubMed PMID: 31364255.
25 Ulum B, Teker HT, Sarikaya A, Balta G, Kuskonmaz B, Uckan-Cetinkaya D, et al. Bone marrow mesenchymal stem cell donors with a high body mass index display elevated endoplasmic reticulum stress and are functionally impaired. J Cell Physiol. 2018;233:8429-36. doi: 10.1002/jcp.26804. PubMed PMID: 29797574.
26 Kim SH, Kim JY, Park SY, Jeong WT, Kim JM, Bae SH, et al. Activation of the EGFR-PI3K-CaM pathway by PRL-1-overexpressing placenta-derived mesenchymal stem cells ameliorates liver cirrhosis via ER stress-dependent calcium. Stem Cell Res Ther. 2021;12:551. doi: 10.1186/s13287-021-02616-y. PubMed PMID: 34689832; PubMed Central PMCID: PMCPMC8543968.
27 Psaraki A, Ntari L, Karakostas C, Korrou-Karava D, Roubelakis MG. Extracellular vesicles derived from mesenchymal stem/stromal cells: The regenerative impact in liver diseases. Hepatology. 2022;75:1590-603. doi: 10.1002/hep.32129. PubMed PMID: 34449901.
28 Du X, Li H, Han X, Ma W. Mesenchymal stem cells-derived exosomal miR-24-3p ameliorates non-alcohol fatty liver disease by targeting Keap-1. Biochem Biophys Res Commun. 2022;637:331-40. doi: 10.1016/j.bbrc.2022.11.012. PubMed PMID: 36423379.
29 Rong X, Liu J, Yao X, Jiang T, Wang Y, Xie F. Human bone marrow mesenchymal stem cells-derived exosomes alleviate liver fibrosis through the Wnt/beta-catenin pathway. Stem Cell Res Ther. 2019;10:98. doi: 10.1186/s13287-019-1204-2. PubMed PMID: 30885249; PubMed Central PMCID: PMCPMC6421647.
30 Mardpour S, Hassani SN, Mardpour S, Sayahpour F, Vosough M, Ai J, et al. Extracellular vesicles derived from human embryonic stem cell-MSCs ameliorate cirrhosis in thioacetamide-induced chronic liver injury. J Cell Physiol. 2018;233:9330-44. doi: 10.1002/jcp.26413. PubMed PMID: 29266258.
31 Chen YX, Zeng ZC, Sun J, Zeng HY, Huang Y, Zhang ZY. Mesenchymal stem cell-conditioned medium prevents radiation-induced liver injury by inhibiting inflammation and protecting sinusoidal endothelial cells. J Radiat Res. 2015;56:700-8. doi: 10.1093/jrr/rrv026. PubMed PMID: 26070321; PubMed Central PMCID: PMCPMC4497399.
32 Gonzalez-Rodriguez A, Mayoral R, Agra N, Valdecantos MP, Pardo V, Miquilena-Colina ME, et al. Impaired autophagic flux is associated with increased endoplasmic reticulum stress during the development of NAFLD. Cell Death Dis. 2014;5:e1179. doi: 10.1038/cddis.2014.162. PubMed PMID: 24743734; PubMed Central PMCID: PMCPMC4001315.
33 Lin D, Chen H, Xiong J, Zhang J, Hu Z, Gao J, et al. Mesenchymal stem cells exosomal let-7a-5p improve autophagic flux and alleviate liver injury in acute-on-chronic liver failure by promoting nuclear expression of TFEB. Cell Death Dis. 2022;13:865. doi: 10.1038/s41419-022-05303-9. PubMed PMID: 36224178; PubMed Central PMCID: PMCPMC9556718.
34 Yang B, Yang X. Mesenchymal stem cell-derived exosomes are beneficial to suppressing inflammation and promoting autophagy in intervertebral disc degeneration. Folia Morphol (Warsz). 2024;83:102-12. doi: 10.5603/FM.a2023.0021. PubMed PMID: 36967623.
35 Park M, Kim YH, Woo SY, Lee HJ, Yu Y, Kim HS, et al. Tonsil-derived mesenchymal stem cells ameliorate CCl4-induced liver fibrosis in mice via autophagy activation. Sci Rep. 2015;5:8616. doi: 10.1038/srep08616. PubMed PMID: 25722117; PubMed Central PMCID: PMCPMC4342568.
36 Hua D, Ju Z, Gan X, Wang Q, Luo C, Gu J, et al. Human amniotic mesenchymal stromal cells alleviate acute liver injury by inhibiting the pro-inflammatory response of liver resident macrophage through autophagy. Ann Transl Med. 2019;7:392. doi: 10.21037/atm.2019.08.83. PubMed PMID: 31555706; PubMed Central PMCID: PMCPMC6736825.
37 Wang Y, Wang JL, Ma HC, Tang ZT, Ding HR, Shi XL. Mesenchymal stem cells increase heme oxygenase 1-activated autophagy in treatment of acute liver failure. Biochem Biophys Res Commun. 2019;508:682-9. doi: 10.1016/j.bbrc.2018.11.146. PubMed PMID: 30528392.
38 Hu C, Zhao L, Zhang L, Bao Q, Li L. Mesenchymal stem cell-based cell-free strategies: safe and effective treatments for liver injury. Stem Cell Res Ther. 2020;11:377. doi: 10.1186/s13287-020-01895-1. PubMed PMID: 32883343; PubMed Central PMCID: PMCPMC7469278.
39 Watanabe T, Tsuchiya A, Takeuchi S, Nojiri S, Yoshida T, Ogawa M, et al. Development of a non-alcoholic steatohepatitis model with rapid accumulation of fibrosis, and its treatment using mesenchymal stem cells and their small extracellular vesicles. Regen Ther. 2020;14:252-61. doi: 10.1016/j.reth.2020.03.012. PubMed PMID: 32455155; PubMed Central PMCID: PMCPMC7232114.